Relations between Synthesis and Microstructural Properties of Copper/Zinc Hydroxycarbonates

Bettina Bems,[a] Michael Schur,[a] Alina Dassenoy,[a] Heinz Junkes,[a] Daniel Herein,[b] and Robert Schlögl*[a]

Abstract: Cu/Zn Hydroxycarbonates obtained by co-precipitation of Cu^{2+} and Zn^{2+} with Na_2CO_3 have been investigated regarding phase formation and thermal decomposition in two series with varying Cu/Zn ratios prepared according to the decreasing pH and constant pH method. Hydrozincite, aurichalcite and (zincian)-malachite were found to form at differing Cu/Zn ratios for both series. For the constant pH preparation the Cu/Zn ratio in zincian-malachite was close to the nominal values whereas excess values were found for the decreasing pH samples. The degree of crystallinity as well as the thermal decomposition temperatures were lower for the constant pH series. All samples containing aurichalcite revealed an unexpected decomposition step at high temperatures evolving exclusively CO_2. The differences in composition and microstucture were traced back to the different pathways of solid formation for the two preparation methods. Substantial changes were observed during the post-precipitation processes of ageing and washing. The effects were studied in detail on samples with a cation ratio of Cu/Zn 70:30 mol %. Ageing of the precipitates in their own solutions is accompanied by a spontaneous crystallization of the initially amorphous solids. The decreasing pH sample develops from a hydroxy-rich material comprising basic copper nitrate (gerhardtite) as an intermediate. Only small changes in the chemistry of the samples were detected for the constant pH precipitation. The findings are summarised into a scheme of solid formation processes that explains the phenomenon of a "chemical memory" of the precipitates when they are converted into Cu/ZnO model catalysts.

Keywords: copper · hydroxycarbonates · precipitation · thermal analysis · zinc

Introduction

Copper/zinc oxide based catalysts are of industrial importance for methanol synthesis and reforming as well as for the water-gas shift reaction. It is widely accepted that ZnO plays a pivotal role in obtaining and maintaining the active copper metal in optimal dispersion. The high activity of this particular system is believed to result from a strong interaction of the two phases leading to a specific quality of the active copper material the nature of which is a matter of discussion.[1] The major hypotheses include synergistic effects from a solid solution of Cu in ZnO,[2] morphological changes of the copper particles[3] or their surface,[4] and Cu/Zn alloy formation.[5] In addition, the presence of residual carbonate in the calcined precursors is known to play an important role achieving active catalysts possibly through subsequent formation of copper suboxide species.[6]

Mixed copper/zinc hydroxycarbonates are well-established precursors for the synthesis of these catalysts. One of the reasons for the ongoing research concerning the chemical and structural identity of these precursors is the presumed conjunction to the activity of the final catalyst, in other words the "memory" of the catalyst of its origin.[7, 8] Figure 1

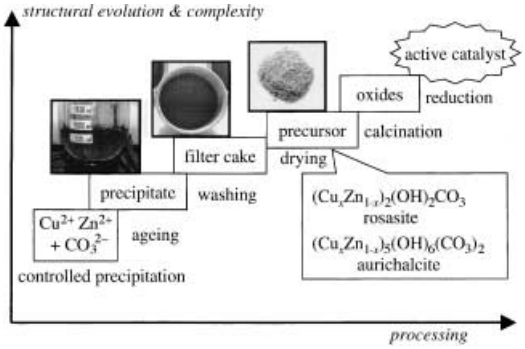

Figure 1. Scheme of the preparation procedure for Cu/ZnO catalysts via hydroxycarbonate precursors.

[a] Prof. Dr. R. Schlögl, B. Bems, Dr. M. Schur, A. Dassenoy, Dipl. Ing. H. Junkes
Fritz Haber Institut of the Max Planck Gesellschaft
Department of Inorganic Chemistry
Faradayweg 4–6, 14195 Berlin (Germany)
Fax: (+49) 30-8413-4401
E-mail: acsek@fhi-berlin.mpg.de

[b] Dr. D. Herein
Institut für Angewandte Chemie Berlin-Adlershof e.V.
Richard-Willstätter-Strasse 12, 12489 Berlin (Germany)

 DOI: 10.1002/chem.200204122

illustrates the typical preparation route of the catalyst via the hydroxycarbonate route. It shows the multistep procedure where each treatment subsequently adds to the structural characteristics of the catalyst finally obtained. Microstructural properties such as size and strain of copper crystallites are traceable throughout the calcination to CuO/ZnO and reduction to the final catalyst as a function of the Cu/Zn ratio.[9] These properties in turn correlate to the activity of the catalyst and corroborate the assumption that copper surface area is not the only parameter determining catalytic activity and bulk structural properties may be of importance.

Investigations on the precursors have been widely limited to analyses of the phase composition whereas other microstructural features such as compositional and structural disorder or particle sizes were only rarely considered. Moreover, comparative studies on the effects of various synthesis procedures often lack detailed information on reaction parameters and statements found in the literature regarding the influence of preparation conditions are often contradictory.[10–14]

Several crystalline phases are known to occur in the precipitates termed according to their mineral analogues; their names will be used throughout this paper. Among them are $Cu_2(OH)_2CO_3$ (malachite) which is capable to substitute up to 30% of Cu by Zn $(Cu,Zn)_2(OH)_2CO_3$ (zincian-malachite) and is then named rosasite, $(Cu,Zn)_5(OH)_6(CO_3)_2$ (aurichalcite) and $Zn(OH)_6(CO_3)_2$ (hydrozincite). In addition, from the nitrates used as metal sources, $Cu_2(NO_3)(OH)_3$ (gerhardtite) is a relevant compound.

Few investigations deal with the processes taking place during and after the precipitation and their effects on catalytic properties. The influences of copper/zinc ratio,[10] precipitation rates, concentration of the solutions[11] as well as the known, however controversially discussed effect of ageing[12, 13] indicate the importance of kinetic factors. The structural characteristics of the solids on various scales such as particle sizes and shapes, degree of agglomeration, epitaxy and intergrowth, chemical and structural disorder are under kinetic control and will be reflected in the behaviour upon calcinations and final catalytic properties. Therefore, it is highly desirable to obtain detailed knowledge about the evolution of the physicochemical properties of the precursors during all preparation steps and their dependence on preparation conditions requiring a chemical insight into the processes of the liquid-to-solid transformation.

One reason for the lacking knowledge which gives the catalyst preparation the image of "black magic" rather than a scientific endeavour is the lack of tools to investigate highly concentrated precursor solutions. This accounts also for the sparsely found calculations of the speciation and thermodynamics. Hence, experimental investigations are often restricted to diluted solutions, which may not well represent the reactions in the practical solid forming procedures.[15, 16]

Being aware of the difficulties associated with ex situ analysis, it is believed that a detailed systematic study still yields valuable information. The present paper compares precipitates with varying Cu/Zn content obtained by different precipitation modes conducted under strictly controlled conditions. It focuses on the effects of the post precipitation procedures of ageing and washing on the thermal decomposition modelling calcination monitored by thermogravimetry (TG) and evolved gas analysis (EGA).

The purpose of this study is to investigate the inorganic chemical reaction sequence leading to the binary hydroxycarbonate. Technical catalysts contain as promoter substantial amounts of aluminium. The role of this addition that increases and stabilises catalytic performance can only be investigated upon a firm knowledge of the chemistry of the binary system. Hence the development of better catalysts is not the emphasis of this work rather than the rationalisation of the complex network of synthesis parameters that controls the performance of the final catalyst.

Results

Comparison of different precipitation modes: Two series of samples with molar Cu/Zn ratios varying from 100:0 to 0:100 in steps of 10 mol% were prepared with the commonly used constant pH and the decreasing pH methods, respectively, whereupon all other parameters were kept constant. In the following the samples are designated according to the scheme n-*xx*/*yy*, where n is the letter indicating the method of precipitation (c or d) and *xx* and *yy* give the nominal molar quantities of Cu and Zn.

Elemental analysis by AAS confirms that the ratio as well as the total amount of Cu/Zn within these samples agrees well with the values used for the preparation and those derived from the phase composition elucidated by XRD within <2% as listed in Table 1. An excess of 3 mol% Cu is observed, however, in the samples d-30:70 and d-40:60. The samples up to 40% Cu show a pronounced increase in the total amount of Cu and Zn despite the expected decrease assuming an ideal stoichiometry of $(Cu,Zn)_5(OH)_6(CO_3)_2$ indicating an excess of hydroxide counterions. Lower contents of Na impurities are found for the constant pH series than for the decreasing pH series. In the former the Na contents are nearly constant at a level of $0.07(\pm 0.02)$ weight% in contrast to an average value of $0.13(\pm 0.04)$ weight% for the decreasing pH series.

The X-ray diffraction patterns of the two series presented in Figure 2 show three different crystalline phases, namely hydrozincite, aurichalcite and malachite/rosasite that occur at characteristic Cu/Zn ratios. The zinc-rich samples up to the

Table 1. Results of AAS determination of cationic contents given in weight% of the two series of Cu/Zn hydroxycarbonates.

Cu/Zn	$Cu_{const.\ pH}$	$Zn_{const.\ pH}$	$Cu_{decr.\ pH}$	$Zn_{decr.\ pH}$
100:0	55.96	0	56.29	0
90:10	50.7	5.98	50.41	6.04
80:20	45.17	11.76	45.42	11.74
70:30	39.11	17.33	39.81	17.59
60:40	33.92	23.5	35.98	22.58
50:50	28.84	29.5	28.48	30.31
40:60	23.27	36.07	25.44	34.17
30:70	17.29	41.22	19.58	39.72
20:80	11.49	46.95	10.7	47.67
10:90	5.42	51.83	5.13	52.61
0:100	0	58.4	0	56.85

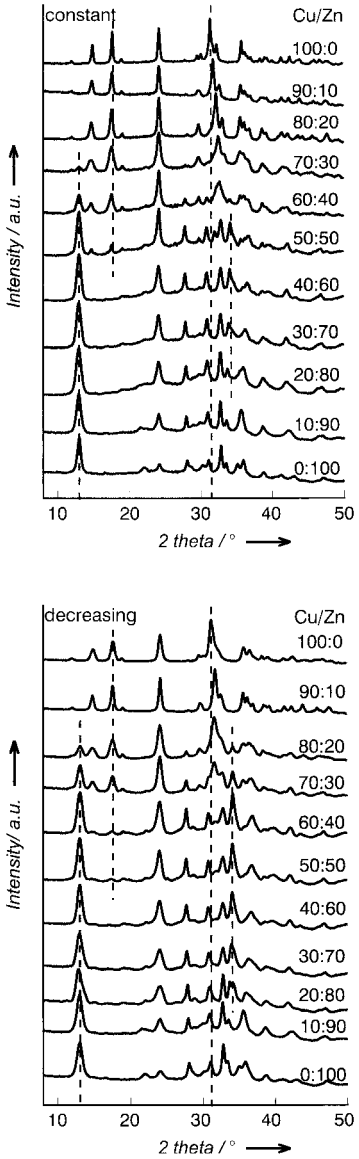

Figure 2. XRD patterns of the dry precursors prepared according to the constant pH (top) and decreasing pH method (bottom).

parity of Cu and Zn comprise hydrozincite and aurichalcite evident by the strong 200-reflection at 13° 2Θ. A distinction between these two phases is accomplished by the strong 121-reflection from aurichalcite at 34° 2Θ occurring at 20 mol% Cu. When the composition exceeds 50 mol% Cu, rosasite is found and with increased copper contents its proportion rises to yield monophasic rosasite/malachite. The biphasic intermediate region will be referred to as transition region. For the decreasing series this region extends towards a higher copper proportion of 80 than 70% for the constant pH series. The observations underline the strong effect of kinetics on the phase formation disregarding the notion that the composition of the precursor solution solely determines the properties of the solid.

The transition region is characterized by high background contributions to the XRD patterns, which indicate the presence of considerable amounts of amorphous material. These contributions are differently pronounced in the two series. The samples c-60:40 through c-20:80 show a modulation of the background with a broad maximum around 33° 2Θ ($d = 2.7$ Å) that is less notable in the decreasing pH series. The nonuniform backgrounds together with the considerably broadened and severely overlapping reflections prevent a full pattern analysis.

Despite these limitations the relative amounts of the crystalline phases were estimated based on the peak areas of the strongest reflections. Figure 3 shows the diagram of states obtained and reveals significant differences between the two series. Aurichalcite is more prominent in the decreasing pH series. In the constant pH series substantial amounts of hydrozincite are observed. The transition region starts with minor amounts of rosasite and strongly increases at characteristically different Cu/Zn ratios (50:50 for the c-series and 70:30 for the c-series) for both series. Aurichalcite persists at higher copper loadings in the decreasing pH series.

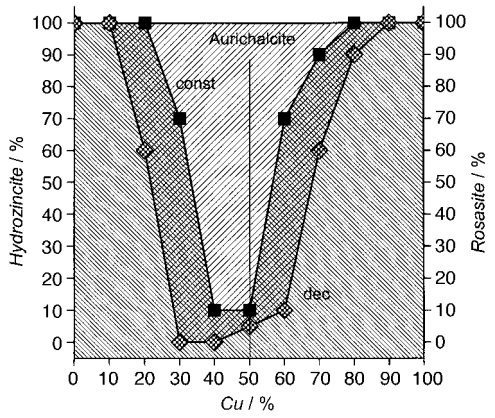

Figure 3. Diagram of state for the constant pH and decreasing pH series showing the proportions of aurichalcite to rosasite (right) and of auricalcite to hydrozincite (left).

Apart from the differences in phase composition other features differ in the powder patterns for samples with the same Cu/Zn ratio within the two series. All constant pH samples exhibit smaller peak profiles indicating larger and/or less distorted crystallites. A continuous increase of the peak width of the rosasite reflections with increasing zinc content occurs only within the c-series. An estimation of the domain sizes with the Scherrer equation (intrinsic profile breadth = 0.1° 2Θ) based on the full width at half maxima (FWHM) of the three strongest non-overlapping reflections (020, 120 and 220) of malachite/rosasite yields a decrease from 35 (5) nm to 11(1) nm for c-100:0 to c-70:30 but only a slight decrease from 12.5 (1) nm to 11(1) nm for the corresponding samples of the d-series. In contrast, the peak width of the 200-reflections of aurichalcite shows only negligible variations around 11(10) nm within both series.

The increasing zinc contents cause shifts of particular reflections from rosasite (see Figure 3). The most pronounced change occurs for the -201-reflection at 31.2° 2Θ shifting to higher angles. A continuous displacement from 31.30° 2Θ to 32.40° 2Θ is found for copper contents of 100% down to 70% in the c-series. Sample d-90:10 exhibits the same shift as the constant pH sample whereas for the following samples no

further downshift is observed. These shifts are correlated to the Cu/Zn ratio of rosasite. An evaluation of the d_{-201}-spacings from rosasite with the data given by Porta[17] for the degree of substitution by Zn reveals a cationic composition close to the nominal Cu/Zn ratio for the c-series. In contrast, the d-samples with nominal composition 90:10 to 70:30 exhibit the same composition of Cu/Zn 85:15 as shown in Figure 4.

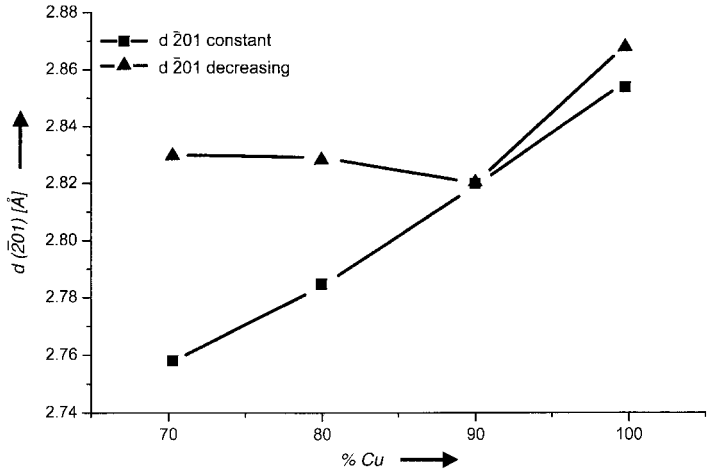

Figure 4. Plot of the d spacings of the $\bar{2}$01 reflections of rosasite versus Cu/Zn ratio from the constant pH and decreasing pH series.

The XRD patterns of hydrozincite reveal shifts of the 002-reflections towards lower d values with increased Cu content of the samples. A decrease from 268 pm in the pure hydrozincite samples to 265 pm at composition 30:70 is detected. A slight shortening (ca. 1 pm) of the axial bonds of the octahedral Zn sites may account for this effect caused by substitution with copper.[18] For a comparison of the relevant geometries of both structures see Figure 5. The nearly equal shifts within both series indicate an equal degree of substitution. Aurichalcite exhibits small shifts of the 121-reflections to higher d values that finally overlap with the 002-reflections from hydrozincite indicating a substitution with zinc. A possible anionic disorder that is the substitution of carbonate by hydroxide would result in a change of the d spacing of the sheets stacked along the *a* axis that is not observed.

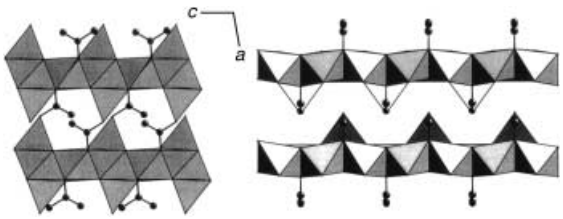

Figure 5. Comparison of the crystal structures of hydrozincite (left) and aurichalcite (right). In both compounds edge-linked octahedra form infinite layers in the *c*,*b* plane with the axial ligands pointing along the [101] direction. Their shortening by substitution of Zn with Cu in hydrozincite is assumed to cause the observed shifts of the 002 reflections. Note, that a decrease in *h*00 spacing is not feasible due to the rigid assembly of the interlayer carbonate groups.

We note that other microstructural features such as positional cation/anion disorder, inhomogeneous composition, or intergrowth between auricalcite and hydrozincite are not accessible by this XRD approach. XRD clearly indicates by the non-proportional variation in the composition of the crystalline solids with the composition of the synthesis solution (see shape of the state diagram) that the solid formation is an incongruent process requiring additional control variables besides the cation ratio.

Thermal decomposition is analyzed in detail as it models the calcination step in the catalyst synthesis (see Figure 1) and yields invaluable information about the anion disposition in the solid when coupled to EGA. The mass losses upon thermal decomposition for the two series are depicted in Figure 6. Slightly higher values are found than calculated from the XRD phase analysis. This is attributed to incorporation of

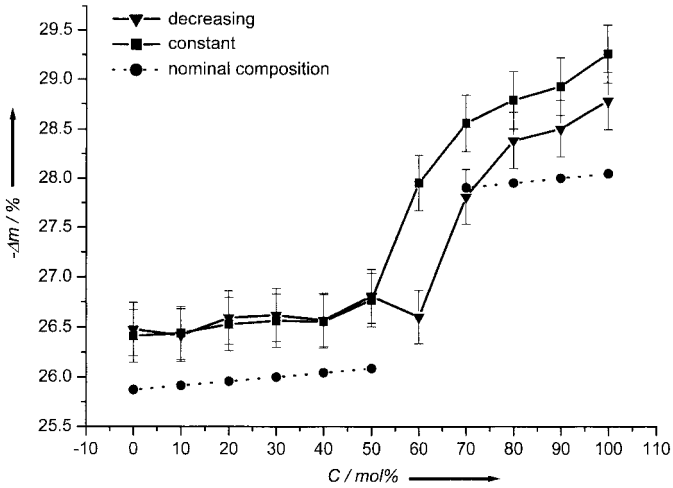

Figure 6. Weight losses upon thermal decomposition for the constant pH and decreasing pH series with varying Cu/Zn ratio. For comparison, calculated weight losses are shown for phase pure hydrozincite/aurichalcite (left array) and rosasite/malachite (right array) with the same cation ratios.

water. The variation with Cu content is in agreement with the abundance of the crystalline phases derived from XRD. No deviations occur within the two series for the zinc-rich samples and the different progressions of the aurichalcite–rosasite transition are clearly reflected in the TG data. Interestingly, sample d-60:40 exhibits a significant lower weight loss than expected from XRD data, where a small amount of rosasite is already visible. This indicates an excess of hydroxide in the anionic composition. The weight losses of the copper richest c-samples are markedly higher than for the d-series indicating higher proportions of carbonate contained in the c-samples. Moreover, the weight losses for both end-members consisting of pure malachite show a small, but significant additional rise. Quantitative EG analysis (see below) suggests that this is due to additional water possibly occluded within the crystals. Due to the obvious deviations from ideal compositions and the very similar weight losses expected for rosasite and aurichalcite the amounts of these phases within the transition region were not quantified based on the TG values.

The DTG traces depicted in Figure 7 show the variations with Cu/Zn ratio and with precipitation procedure. The monometallic samples reveal a well-defined single decomposition step. The incorporation of the second metal leads to a stabilization of malachite and hydrozincite, respectively, as evidenced by the shift of the DTG peaks from about 250 to 350 °C. A concomitant broadening of the peaks, however, indicates an increasing inhomogeneity of the materials. The peak temperature of c-80:20 exhibits a pronounced shift in contrast to the decreasing sample in agreement with the different cationic ratios in rosasite from both series. The generally higher temperatures for the maximum decomposition rates of the constant pH samples are attributed to the larger crystallite sizes of this series. The decomposition patterns become more complex with the presence of the second phase aurichalcite as apparent in particular for the constant pH samples. These materials decompose in a range from below 150 up to 500 °C.

A remarkable feature is the well-resolved decomposition step at temperatures between 380–500 °C emerging for compositions 30:70 through 70:30 and recognizable for samples with composition 20:80 and 80:20. The maxima of these peaks vary between 440 and 480 °C with the highest values obtained for the copper-richest samples. As these decomposition temperatures are above the calcination temperatures of catalysts, the species causing this feature will persist in activated catalytic systems.

Evolved gas analysis (EGA) of H_2O and CO_2 provides a more detailed picture of the decomposition process. The EGA-traces for CO_2 shown in Figure 8 confirm the distinction of two qualitatively different decomposition steps. Water and CO_2 are released simultaneously in the first step for which reason the water traces are not shown. The high-temperature decomposition step is exclusively due to the release of CO_2. According to the high temperature resistance of this carbonate species it will be referred to as HT-CO_3.

The decomposition patterns for the zinc-rich samples up to the composition 40:60 are almost identical for both series with

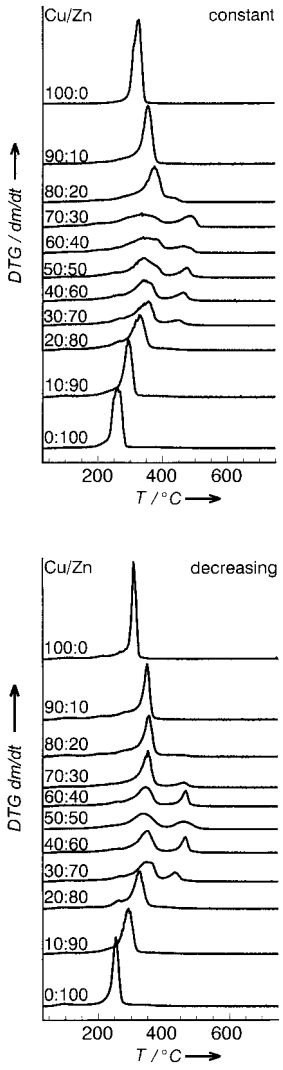

Figure 7. DTG traces during thermal decomposition for the constant pH (top) and decreasing pH (bottom) series.

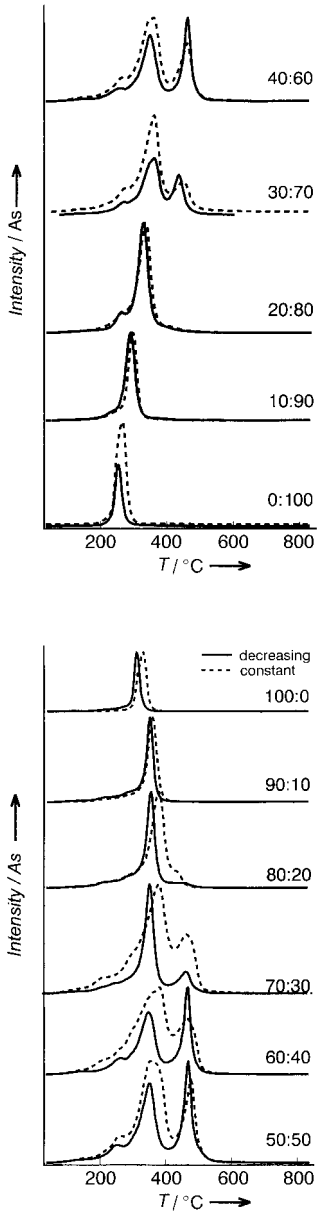

Figure 8. CO_2-EGA traces of the constant pH and decreasing pH series during thermal decomposition upon heating at 10 K min^{-1}.

a smooth trend of succeeding samples confirming the close relationship of the two phases. A distinct second peak at lower temperatures for the first decomposition step and, simultaneously, the high temperature carbonate species is observed starting from 20% Cu in parallel with the occurrence of aurichalcite. This pattern is characteristic for all samples containing aurichalcite that are samples d-50:50 to d-70:30. In contrast, the corresponding samples c-60:40 and c-70:30 display more complex and poorly resolved decomposition patterns in agreement with the large abundance of the transition phase (see Figure 3).

The results of the quantification of the EGA traces are shown in Figure 9. The anionic composition of hydroxide and carbonate is calculated as mmol g^{-1} $M(OH)_2$ and $M(CO_3)$ using the mean molar weight M according to the ratio of the metals. The overall trend confirms the phase composition detected by XRD. However, distinct deviations are observed.

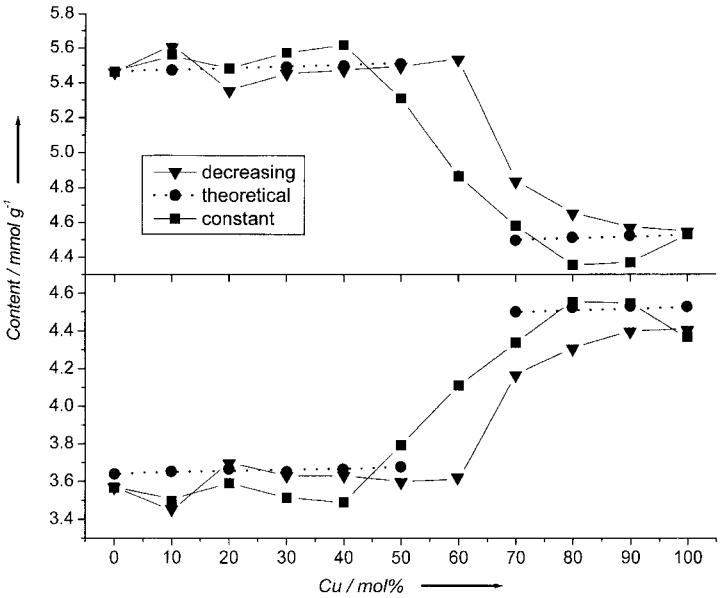

Figure 9. Anionic composition given as mmol $M(OH)_2$ and MCO_3 (M is the respective mean molar weight of the metals of the two series as determined by quantitative EGA). For comparison, calculated values for phase pure samples are included.

For the zinc-rich region a weak trend towards increasing proportions of hydroxide with increasing Cu content is observed. Both series exhibit a discontinuity with an excess of hydroxide between 10 to 20% Cu where aurichalcite starts to form. The constant pH samples up to the transition region display slightly lower contents in carbonate than the decreasing pH samples. The transition regions are characterized by different progressions of the change in the chemical composition. For the constant pH series an almost linear increase of the hydroxide to carbonate ratio is observed whereas the decreasing series exhibits an asymptotic progression. The special character of the sample d-60:40 is reflected in the anionic composition expected for pure aurichalcite although XRD analysis indicates the presence of rosasite. The proportion of carbonate is lower for the copper rich samples d-80:20 and d-90:10 in agreement with the TG results resulting in a deficiency in carbonate compared with stoichiometric compositions. Both malachites again comprise the same anionic composition.

Different proportions of the high temperature carbonate based on the total amount of CO_2 released are obtained for the two series as shown in Figure 10. The general progression with the content of Cu correlates to the amount of aurichalcite with a plateau from 40 to 60% Cu. The amounts of HT-CO_3 are significantly lower for the constant pH samples in this

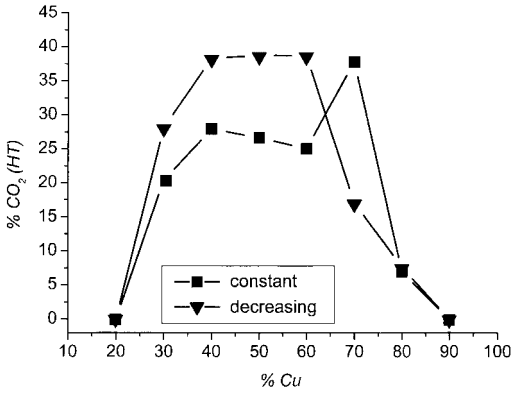

Figure 10. Proportions of CO_2 released in the high temperature decomposition step as a function of the amount of Cu and method of precipitation.

compositional range. However, sample c-70:30 exhibits a significantly higher value than the corresponding decreasing pH sample. The occurrence of the high temperature carbonate species seems to be related to the presence of aurichalcite, but there is an additional factor correlating the two entities. To check whether the high temperature carbonate is an inherent feature of aurichalcite, handpicked large grown natural crystals were analyzed as a reference.[19] This well-crystalline material exhibits only one sharp decomposition step with a maximium rate at 402°C. Either an additional phase related to aurichalcite or kinetic hindrance of some occluded carbonate (at the phase boundary between resulting Cu oxides and ZnO) account for the HT-CO_3 species. In this context it is interesting to note that $ZnCO_3$ (smithonite) decomposes between 400 and 600°C.

Simultaneous monitoring of the heat flows upon thermal treatment shows that all decomposition steps are accompanied by endothermic events. The first decomposition step gives pronounced signals whereas the second signal is about two orders of magnitudes weaker. The second event is succeeded in the majority of cases by a likewise weak exothermic event indicating crystallization. The heat flows for the first step scatter irregularly around 500($\pm$100) J g^{-1} for both series. Evaluation of the values for the second step is hampered by their small magnitudes and the overlap with the exothermic event. In Figure 11 the magnitudes for the exothermic events are shown. A maximum is observed for the copper/zinc ratio of 50:50 for both samples. In general, for the constant pH samples significantly lower values are found which come close to zero for copper contents higher than 50%. It is assumed that in these cases at least part of the

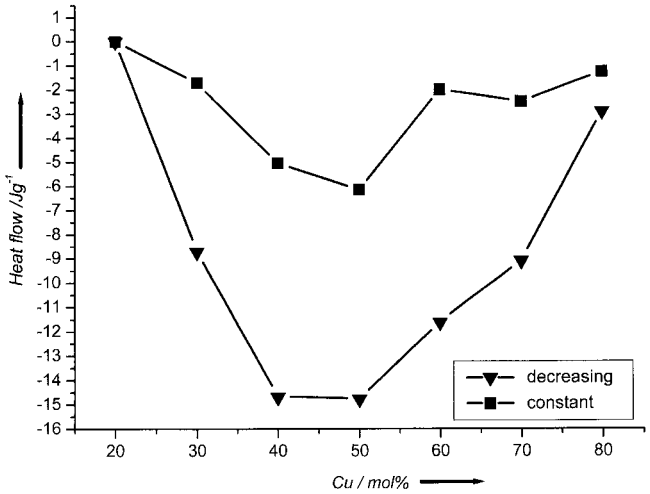

Figure 11. Comparison of the integrated heat flows for the crystallisation process (exothermic) after thermal decomposition of the hydroxycarbonates from both series.

crystallization occurs simultaneously with the endothermic release of the gaseous compounds thus obscuring the latter.

Effects of ageing and washing: For the investigation of the changes during the post-precipitation treatments samples with the cation ratio of 70:30 were chosen due to the relevance of this composition for catalyst preparation.[20]

The different evolutions of the pH value during ageing of the samples from the constant pH series depending on the Cu/Zn ratio are depicted in Figure 12. A striking feature is an instant drop of 0.1 to 0.2 pH units occurring after various induction times in the composition range from 40:60 to 90:10 followed by a somewhat slower increase up to the initial value. For the decreasing series similar but less pronounced events were observed only for the compositions 70:30 and 80:20 (not shown). The copper-rich samples c-90:10 and c-80:20 exhibit a sharp drop whereas the decrease in pH is broadened for

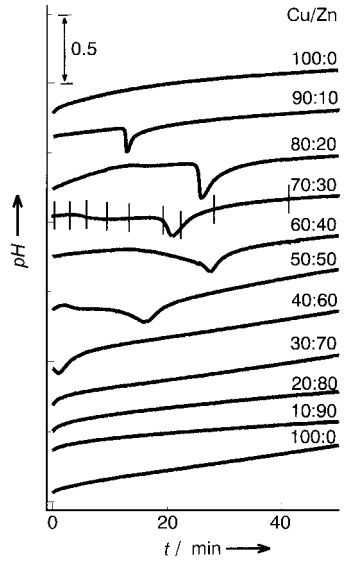

Figure 12. Evolution of pH during ageing of precipitates of the constant pH method. The bars mark the points in time where specimens were taken for further characterization.

samples containing more zinc indicating less defined and/or slower rates of the transformation process involved. The period until minimum pH is reached lasts approximately 25 minutes for 60 up to 80% Cu and is markedly shorter for the other compositions. A long term continuous increase of 0.5 to 1 pH units within 120 minutes of ageing from the starting pH 7 was noticed that is due to the continued incorporation of carbonate into the solid releasing hydroxide.

To verify the origin of the pH drop and the effect of ageing, specimen were isolated during the ageing of a c-70:30 precipitate at intervals of approximately three minutes during the first 30 minutes and at intervals of several hours up to 18 hours. The XRD data shown in Figure 13 reveal that the

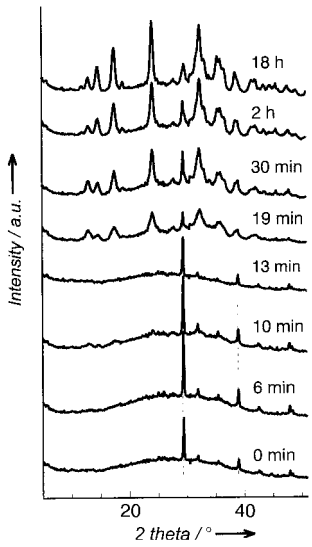

Figure 13. XRD patterns of differently aged samples of a precipitate with cation ratio Cu/Zn 70:30 prepared according to the constant pH method.

initial precipitate is amorphous exhibiting only the peaks of admixed $NaNO_3$ with the indicative strong reflection at 29° 2Θ. Crystallization of rosasite and aurichalcite starts simultaneously coinciding with the pH drop corroborating that this effect is a direct indicator for the transformation of the solid. The positions of the reflections do not shift with ageing and after 30 minutes no further alterations of their shapes are observed showing that crystal growth has terminated. The amount of aurichalcite decreases to 50% of the initial value within the first three hours of ageing as evidenced by the progression of the intensities of the 002-reflection indicating that the system then has reached a stable state.

IR spectra of the samples were recorded as shown in Figure 14 in order to examine the changes of the local environments of the anions. The data confirm the spontaneous crystallization process. The patterns of the samples taken within the first 13 minutes correspond to georgeite which is an amorphous modification of rosasite. The characteristic single band around 837 cm^{-1} is attributed to a wagging vibration of carbonate.[21] The asymmetric C–O stretching vibration is observed at 1400 cm^{-1} with a broad and intense doublet. The symmetric C–O stretching vibration around 1100 cm^{-1} is split into a doublet due to the reduction of symmetry in bonded carbonate and only weakly visible in the

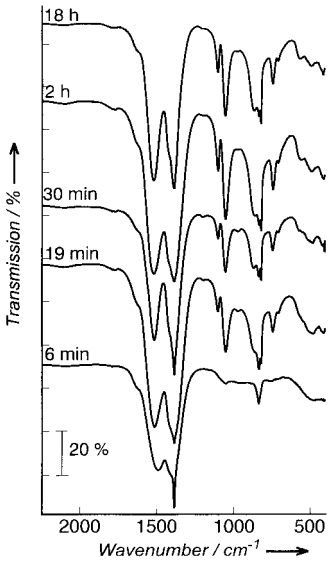

Figure 14. IR spectra (transmission) of precipitates from sample c-70:30 aged for different times as indicated.

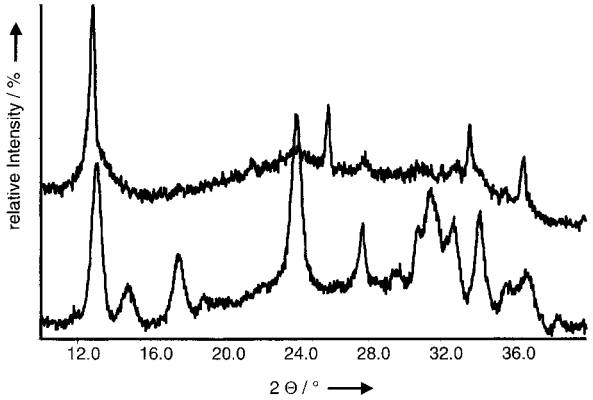

Figure 15. Comparison of XRD patterns of precipitates with cationic ratio Cu/Zn 70:30 aged for 15 minutes (top) and 120 minutes (bottom) prepared by the decreasing pH method.

initial precipitate. After crystallization the intensity is strongly enhanced with no changes in the peak position being observed during ageing. A sharp peak at 1385 cm^{-1} indicative for the asymmetric N–O vibration of nitrate points to an integration of this anion into the solid that is most pronounced for the amorphous samples. All crystallized samples display the spectra of the phases rosasite and aurichalcite with a splitting of the strong doublet around 1400 cm^{-1} and the weak signals at 1200 cm^{-1} (M–OH bending vibration).[22, 23]

To further assess the differences induced by the c and d preparations, samples aged for only 15 minutes—so as not to reach crystallization—are compared with those from the standard 120 minutes ageing. The duration of ageing (i.e., – 15 and 120 min) is given in parenthesis.

The X-ray diffraction patterns of the shortly aged samples exhibit weak and diffuse reflections of aurichalcite and rosasite indicating their commencing crystallization obviously induced during the washing treatment. In contrast to sample c-70:30 (15 min) additional sharp and strong reflections of gerhardtite[24] are found for sample d-70:30 (15 min) as shown in Figure 15.

The IR spectra for the shortly aged samples confirm the differences between both samples. In addition to the georgeite pattern found for c-70:30 (15 min) the decreasing pH sample exhibits very weak signals at 970 and 1200 cm^{-1} indicative for aurichalcite and sharp absorptions at 1385 and 1050 cm^{-1} indicative for gerhardtite.[25]

The evaluation of the anionic composition by EGA reveals a slight enrichment in carbonate for the constant pH method during ageing as shown by the ratio $M(OH)_2/MCO_3$ that drops from 1.2 to 1.1 after 120 minutes ageing. The samples from the decreasing method undergo a pronounced conversion from a hydroxy-rich material to their final composition leading to a change of the $M(OH)_2/MCO_3$ ratio from 1.8 down to 1.3. The abundance of these anions shows that gerhardtite is a minor constituent with less than 20 % weight of the sample. Further, the amount of the HT-CO_3 species strongly decreases during the ageing of the constant pH samples from 37 % after 15 minutes down to 23 % at 120 min.

Washing is evidently applied to remove nitrate occurring as $NaNO_3$ and as gerhardite from the preparation. The presence of nitrate is known to lower the activity of the final catalysts.[26] One detrimental effect is its ability to enhance sintering of the final copper particles. Therefore, the removal of nitrate during washing is of special interest as well as observations on possible structural changes. To this end, the four samples described in the preceding section with a ratio of cations of 70:30 were analysed after each of six repeated washing treatments.

Diffraction analysis shows that the removal of crystalline $NaNO_3$ is complete after the first washing treatment as the strong reflection at 29° 2Θ disappeared. No noticeable variations were found in the diffraction patterns of the hydroxycarbonate phases throughout the washing series. The lowering of the intensities of the reflections from gerhardtite in sample d-70:30 (15 min) indicates that this compound is successively dissolved.

Quantitative EGA similarly shows no significant changes of the anionic composition regarding hydroxide and carbonate throughout all washing series. The EGA patterns, in contrast, display drastic changes upon the repeated washing treatments with exception of sample d-70:30 (15 min). In Figure 16 the typical development is shown for the sample c-70:30 (120 min). The initial precipitates washed only once exhibit a single decomposition step with co-evolution of H_2O and CO_2 occurring in a temperature range from 250 to 310 °C. Sample d-70:30 (120 min) shows a minor presence of HT-CO_3. The second washing leads to a marked shift to higher temperatures for the decomposition as listed in Table 2.

This effect is more pronounced for the constant pH samples shifting from 260 to 350 °C and 320 to 380 °C for the short and long aged samples, respectively, compared with the rise from 310 to 340 °C in sample d-70:30 (120 min). In the subsequent washing treatments only a small rise occurs of these temperatures. The abundance of HT-CO_3 is continuously growing at different rates for the different samples. In addition, a rise of the maximum decomposition temperatures of HT-CO_3 is observed. This general progression is noticeably retarded for

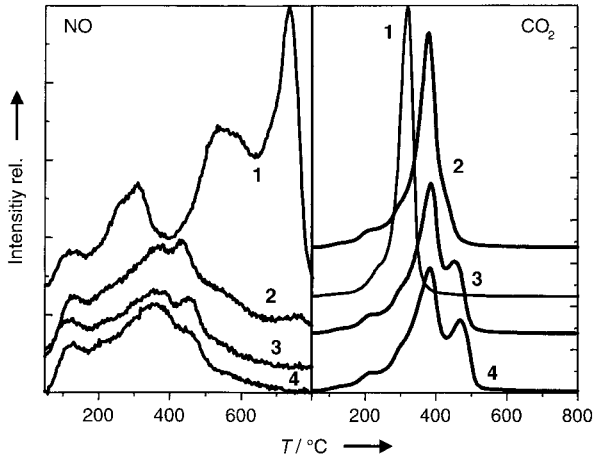

Figure 16. Comparison of the evolution of CO_2 and NO EGA traces for sample c-70:30 (120 min) after repeated washing treatments.

sample c-70:30 (15 min) compared with the long aged samples (Table 2).

The EGA traces of mass 30 (NO) monitor the removal of $NaNO_3$ decomposing at 750 °C as shown in Figure 16. For both long-aged samples the data confirm that the discharge of $NaNO_3$ is essentially complete after the first washing treatment. Only small signals for NO were observed during the decomposition of the hydroxycarbonates, indicating minor amounts of nitrate. Their traces are poorly resolved indicating a form of co-existence with a matrix phase rather than a mixture of defined phases. In contrast, for the short-aged samples noticeable amounts of NO are detected at 750 °C up to the third washing treatment indicating that $NaNO_3$ is probably formed during formation of the hydroxycarbonates occurring with washing. An evolution of mass 30 around 600 °C except for sample d-70:30 (15 min) represents occluded anions evolving after breakdown of the hydroxycarbonate hosts. Sample d-70:30 (15 min) displays a distinct decomposition event for nitrate around 400 °C as shown in Figure 17. Continued washing leads to a downshift of the peak temperature and an intensity increase. Obviously, some NO_3^- is progressively transferred from $NaNO_3$ into the copper/zinc hydroxycarbonates decomposing at lower temperatures. A similar development is observed for sample c-70:30 (15 min) where the decomposition of this additional NO_3^- species eventually coincides fairly well with that of the HT-CO_3 species. However, the extent of transfer is less pronounced. This points towards an incorporation of NO_3^- into amorphous compounds.

Although the decrease of the amount of $NaNO_3$ correlates to the development of HT-CO_3, careful inspection of the traces for mass 30 shows that the two events do not coincide. As shown for sample c-70:30 (120 min) in Figure 16 the HT-CO_3 species emerges after the third washing treatment whereas almost no changes of the NO traces are observed after the first washing treatment and the absence of signals around 750 °C indicates complete removal of $NaNO_3$. This strongly suggests that these two events are independent from each other and HT-carbonate is not introduced during washing. On the other hand, the absence of HT-CO_3 with even minimal amounts of NO_3^- remaining after the second washing indicates that the formation of the HT-CO_3 species is extremely sensitive to the presence of this anion. It is noted that the amounts of $NaNO_3$ initially occluded in the precipitates are significantly lower for the samples with longer ageing. The unexplained negative effect of nitrate impurities on the final catalyst lifetime is rationalised as nitrate inhibiting the formation of the essential HT-CO_3 acting as glue between copper and zinc oxide.

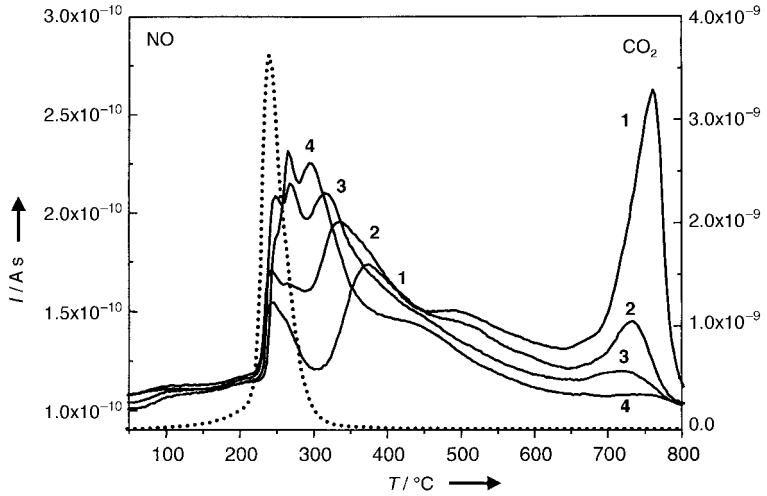

Figure 17. Progression of the release of CO_2 (dotted line, shown only for the first treatment) and NO by EGA for sample d-70:30 (15 min) after repeated washing treatments.

Table 2. Decomposition temperatures and amount of HT-CO3 species for samples aged 15 and 120 min and washed several times.

	T_{peak} [°C] main decomp.				T_{peak} [°C] HT-CO_3 decomp.				[%] HT-CO_3			
	d15	c15	d120	c120	d15	c15	d120	c120	d15	c15	d120	c120
w1	250	260	310	320	–	–	425	–	–	–	11	–
w2	250	325	335	380	–	–	450	–	–	–	17	0
w3	250	340	340	380	–	–	460	450	–	–	17	22
w4	250	350	340	380	–	425	470	475	–	19	18	25
w5	250	350	340	380	–	430	470	475	–	22	18	25
w6	250	350	340	380	–	460	470	475	–	37	18	27

Discussion

The scheme in Figure 18 gives an overview on the variations in preparation and the processing steps that were investigated in this work. The first part is dedicated to the influence of the precipitation method, that is, constant pH or decreasing pH and the variation of the Cu/Zn ratio. In the second part the specific effects of ageing and washing are examined on samples with a cationic ratio Cu/Zn 70:30.

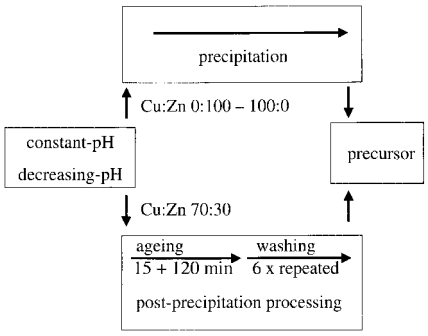

Figure 18. Scheme of the various preparation parameters investigated.

The two precipitation methods primarily result in different phase compositions of the precursors. Application of the decreasing pH method affords higher proportions of aurichalcite throughout the Cu/Zn compositional range that is obviously caused by the more alkaline conditions of this precipitation method favoring hydroxy-rich phases. Furthermore, differing microstructural features namely crystallite sizes and cation distribution as well as varying anionic compositions are obtained. These differences are determined by the differing pathways of formation of the solids during and after the precipitation. The fundamental steps of the presumed pathway of formation for the copper-rich precursors obtained with both preparation methods are summarized in the scheme of Figure 19; The numbers represent the following reactions:

$$Cu(OH)_2 + Zn^{2+} + CO_3^{2-} \rightarrow [(Cu,Zn)_2(OH)_2CO_3]_s \quad (1)$$

$$[M(OH)_x]_s + NO_3^- \rightarrow [M(OH)_{x-1}(NO_3)]_s \quad (2)$$

$$[Cu(OH)_2]_s + OH^- + NO_3^- \rightarrow [Cu_2(OH)_3(NO_3)]_s \quad (3)$$

$$[M_x(OH)_{2x-1}(NO_3)]_s + OH^- \rightarrow [M_x(OH)_{2x})]_s + NO_3^- \quad (4)$$

$$[M_x(OH)_{2x-1}(NO_3)]_s + H_2O \rightarrow [M(OH)_{2x})]_s + HNO_3 \quad (5)$$

$$[M_x(OH)_{2x-1}(NO_3)]_s + HCO_3^- \rightarrow [M_x(OH)_{2x}(HCO_3)(H_2O)]_s + NO_3^- \quad (6)$$

For constant pH samples the sequence of solid formation steps starts with the initial precipitation of amorphous copper hydroxide due to the more acidic character of Cu^{2+} compared with Zn^{2+}. This all-important step of initial solid formation excludes the frequent notion about "co-precipitation" and lays the foundation for the dominance of kinetic effects on the complex sequence of events that are necessary to end at a mixed hydroxycarbonate.

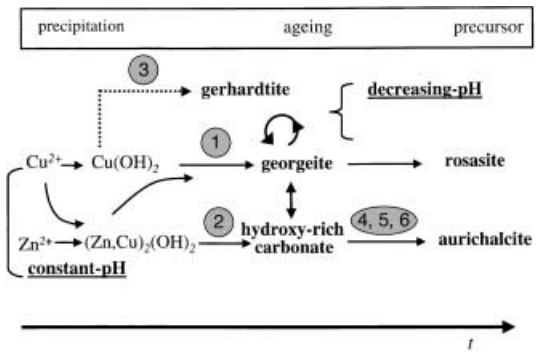

Figure 19. Pathways of solid formation for both preparation methods.

The copper hydroxide then reacts with Zn^{2+} and CO_3^{2-} forming a mixed amorphous hydroxycarbonate (georgeite) as formulated in reaction 1 in Figure 19. This secondary product exhibits the same anionic composition as rosasite. In a concurrent reaction the more slowly solidifying zinc forms a hydroxy-rich material together with the residual Cu^{2+} ions. This material is assumed to incorporate the main fraction of nitrate found in the precursors via reaction 2.

The presence of different species within the initial precipitates is evidenced by the complex thermal decomposition pattern. The small signal preceding the main decomposition is attributed to the hydroxy-rich species. The precursor formation is "incongruent" due to the different kinetics of solid formation for both metals resulting in an intimate phase mix. This gives rise to the complex thermal decomposition pattern and opens the possibility to kinetically control the particles properties of the oxide system resulting from calcinations of the hydroxycarbonate precursor.

The process of precursor formation is not finished with the end of the precipitation phase but clearly continues during ageing and therefore accounts for the importance of the post precipitation handling. The initial solids slowly transform during ageing presumably by partial dissolution/re-precipitation reactions. Two processes are conceivable as indicated by reactions 4 and 5 namely by direct action of hydroxide or through hydrolysis. These processes account for the removal of nitrate and will lead to an intermediate solid enriched in hydroxide. A similar development was observed for the transformation of gerhardtite upon addition of hydroxide or carbonate.[27, 28] Cation exchange during the ripening of the preformed solids cannot be excluded as indicated by the question mark in Figure 19. In addition, carbonate or bicarbonate may likewise be incorporated in a slow reaction by anion exchange (reaction 6).

The reorganization of the solid eventually leads to the formation of nuclei of the two crystalline end-phases rosasite and aurichalcite from either georgeite or the amorphous hydroxy-rich material. The kinetics of these processes clearly depends on the Cu/Zn ratio. The final crystallization proceeds rapidly to the hydroxycarbonates that are intermixed with metastable residues in the compositional range used for catalyst synthesis (transition region in Figure 3). Different growth rates depending on the Cu/Zn ratio may determine the varying crystallite sizes found for rosasite. The evolution of the pH thus is clearly an indicator of the crystallization as

protons result from hydrolysis and from polycondensation reactions. It is presumed that during these processes the primary metal–ligand building blocks remain intact rather than that a complete dissolution and re-precipitation occurs.

The process of solid formation in the decreasing pH procedure is more complex due to the enhanced difference in the precipitation kinetics of the metals. The more alkaline conditions promote the formation of $Cu(OH)_2$ in the first place transforming into copper-rich georgeite according to reaction 1. Simultaneously, under these conditions $Cu(OH)_2$ is susceptible to the reaction with NO_3^- forming gerhardtite as a crystalline intermediate (reaction 3). The rate of this reaction is enhanced by the amphoteric character of zinc that will precipitate at a later stage as compared with the constant pH preparation. Accordingly, less zinc is incorporated forming georgeite and the amorphous hydroxide species forms to a greater extent than in the constant pH preparation that is also enriched in zinc. These factors eventually result in the preferential formation of aurichalcite.

It is emphasized that during the decreasing pH precipitation several regimes of pH are passed that differ in precipitation pathways and kinetics. Gerhardtite reacts upon ageing with carbonate and finally yields rosasite. The transformation of georgeite proceeds as described for the constant pH method. However, the prevalence of hydroxide will enhance the formation of hydroxy-rich intermediates in the initial stages of precipitation resulting in a continuous re-formation of gerhardtite as indicated by the circle in Figure 19. Thus, gerhardtite serves as a storage phase for Cu^{2+} during the crystallization of rosasite from georgeite. The extended nucleation period resulting from this mechanism agrees with the smaller crystallites found for the decreasing pH method. It is further in accordance with the less pronounced pH drop found during ageing of the decreasing pH samples. Since gerhardtite is not known to adopt large amounts of Zn^{2+} and georgeite comprises higher proportions of copper, it follows that Cu is enriched over its nominal abundance in the final crystalline rosasites from the decreasing pH samples (see Figure 4). The proposed pathway of formation with $Cu(OH)_2$ and gerhardtite as intermediates affects in particular the copper-rich samples with a Cu content of 60–80 mol% concerning their phase composition and microstructural features.

Prolonged ageing leads to a loss of aurichalcite for both preparation methods in agreement with earlier reports.[13] No indication was found for an enrichment of rosasite in Zn accompanying the conversion of aurichalcite. This loss of crystalline material to the pool of non-crystalline phase is not observable by XRD due to the very weak signals for noncrystalline solids and their presence in the non-aged samples. The degree and rate of aurichalcite loss are controlled by several factors including crystallite sizes and CO_3^{2-}/HCO_3^- concentration.

A discrepancy to earlier reports on the formation process of the hydroxycarbonates is the absence of sodium zinc carbonate $Na_2Zn_3(CO_3)_4 \cdot 3H_2O$ as an intermediate which was not observed in any of our ageing experiments. This phase has been reported to be a crucial precursor to the zinc-rich hydroxycarbonates.[8, 29] The authors used, however, a higher carbonate to metal ratio than employed in the present study. Sodium zinc carbonate is thus not generally an intermediate in the formation of hydroxycarbonate precursors.

The varying amounts of the high temperature carbonate species is a consequence of the initial abundance of carbonate during the first solid formation and hence correlates with the method of preparation. In the literature HT-CO_3 was attributed to a final decomposition step of aurichalcite forming an oxy-carbonate[30] or to stem from the reaction of the Zn centers in rosasite and to shift its decomposition temperature to higher values with increasing Zn content.[31] The present results associate this species to aurichalcite and more directly to its progenitor, the hydroxy-rich amorphous phase. The varying abundance observed in particular for the samples with a Cu/Zn ratio of 70:30 strongly suggest that an additional factor determines its formation. The amount of interfacial region between auricalcite and its amorphous progenitor is the likely controlling factor. This assumption is corroborated by the trends observed with the washing treatments where EGA clearly shows the modification of the material. It is speculated that the surface of aurichalcite is altered through dissolution re-precipitation processes forming composite or core-shell particles. The smaller crystallites with a total larger interfacial area resulting from the decreasing series would then explain the higher amount of HT-CO_3 for the samples with the Cu/Zn ratio 40:60 through 60:40 compared to the constant pH series.

A consequence of ageing and washing is the reduction of the amount of nitrate in the precursors. This anion exerts a strong adverse effect on the formation of the high temperature carbonate species indicating a reduced particle interface region that leads to the observed effect of CuO sintering during later activation of the precursor. Another effect of ageing is the reduction of the amount of hydroxides. This will affect the crystallite sizes of the resulting copper oxide since the presence of water during the thermal decomposition reduces the chemical potential of oxygen and thus reduces nucleation of oxide. The copper oxide crystallites obtained from copper-rich samples are markedly larger for the decreasing pH series though the crystallites of their precursors are smaller than those of the constant pH series.[9]

The "chemical memory" was traced back to a direct influence of the precursor phases on the structural properties of copper.[9] A strong increase of the microstrain with decreasing copper content was found for the zinc-rich samples.[9, 33] This effect is significantly stronger for the constant pH series and is attributed to the higher amount of (cupper)-hydrozincite providing a greater dispersion of copper than aurichalcite. The development of the crystallite sizes in CuO of the calcined samples follows the same trend as for the precursors for example, a strong decrease with substitution of Zn in the copper-rich samples for the c samples and a smaller one for the d-samples.[9] The c-samples exhibit smaller CuO crystallites, which may be related to the different copper/zinc ratios within the rosasite precursors but the dominant influence is the anionic composition of the precursor controlling directly the nucleation process of the oxides.

The present investigations clearly demonstrate that the process of precursor formation is not finished with the end of

the precipitation. In addition, it is emphasized that the quality of the material being altered in each synthesis and post synthetic modification step directly depends on the conditions of each preceding step giving rise to the memory effect quoted in the introduction. This memory translates further into the calcination and into the final catalyst by the nucleation controlling effect for the oxides of the volatile anions from the precursor.

Conclusion

The detailed analysis of formation and reactivity of the binary hydroxycarbonates confirms the metastable character of the products accounting for the strong influence of the conditions of the precipitation on the nature of the catalyst precursors. The study further stresses the importance of the post-precipitation treatments. It is concluded, that the different phase mixtures obtained with the two preparation methods are caused by the incongruent precipitation reactions of the metals. The kinetics of the respective reactions is controlled by the choice of precipitation conditions. A model is presented for the sequence of events leading to the copper-rich samples. A different effect of the presence of large amounts of zinc cannot be excluded.

The model features two amorphous intermediates representing the progenitors to the crystalline products those form during the ageing. Ageing is thus a key step in the post precipitation process for determining the microstructural characteristics of the products serving as precursor material. The investigation of ageing revealed that transformations and equilibrations take place at different timescales that depend on the foregoing precipitation process. This comprises exchange reactions between the preformed phases and their transformations into crystalline solids. These processes are characterized by a long-term enrichment in carbonate and, in particular for the decreasing pH samples the conversion of nitrate containing phases, that is, gerhardite into hydroxycarbonates.

A key result of our investigations is the identification of the metastable nature of the initially precipitated material. Composition and structure of the fresh precipitate are neither related to stoichiometric expectations nor to the final dry products. The exact determination of the variability of the anionic composition by EGA was a major analytical breakthrough enabling the description of the complex process of precursor formation as claimed in Figure 18.

It is noted that especially the compositional region of relevance for catalytic application is characterized by the transition regime between the phases of aurichalcite and rosasite and therefore is particularly sensitive to the exact conditions of preparation.

One pronounced "memory" item that remains from the preparation is the high temperature carbonate species. EGA is here an exceedingly useful method to monitor this species. EGA is much more sensitive to subtle changes in the microstructure than XRD that has to rely on long-range order. The HT-CO_3 is coupled in its presence to a combination of aurichalcite and a metastable amorphous hydroxycarbonate. Since this species will persist after the typical calcination conditions its presence will result in a modified microstructures not only of the oxides but also of the reduced catalysts. To our knowledge the correlation between preparation conditions and the specific evolution of the high temperature carbonate species has not been issued before.

An illustration of the relevant microstructural features of the precursor materials with respect to the final properties of the calcined oxides is presented in Figure 20. It is noted that

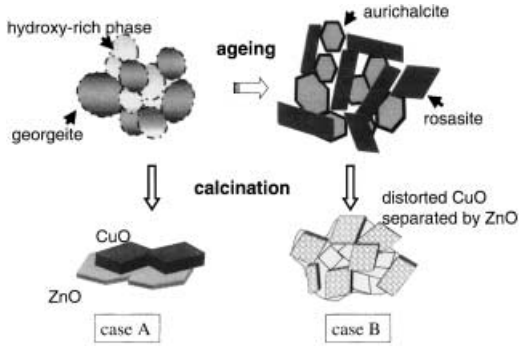

Figure 20. Evolution of microstructural characteristics with ageing of the precursors and the resulting oxides.

the resulting catalyst cannot be regarded as being "supported" by ZnO due to the mass ratio of Cu to Zn.[3] The primary catalyst particles are approximately equally sized oxide particles exhibiting a substantial solid–solid interface. The geometry of the interface and the internal microstructure of both components will result from the peculiarities of the precursor. The amorphous and therefore more reactive precursor with high hydroxide and nitrate contents allows the growth of well-separated large CuO and ZnO crystallites whereas a finely granular and crystalline precursor produces an intimate intergrowth of small and distorted oxide crystallites. It is speculated that the amorphous components form during calcinations a kind of "ZnO boundary". In this context, the HT-CO_3 may additionally serve as growth inhibitor for the oxide crystallites.

This study has laid the foundation of a concise chemical description of the liquid-to-solid transition of a catalyst precursor. Even without taking into account the practically relevant presence of a third cation (aluminium) it is possible to explain several "magic" effects such as time effects during precipitation and post-precipitation handling, color changes and the mode of addition of the reactants on the final catalyst. The translation of the present findings into the later stages of calcinations and activation was investigated in detail with in situ structural methods.[9, 32, 33] The work reveals the importance of "standard aqueous chemistry" for the science of catalytic materials. The study is an illustration of what chemistry is to be known in detail in order to enable a controlled or even "designed" synthesis of a catalytic functional material with practically relevant methods.

Experimental Section

In the decreasing pH method the metals dissolved in nitric acid are added to a solution of sodium carbonate whereas simultaneous mixing of the

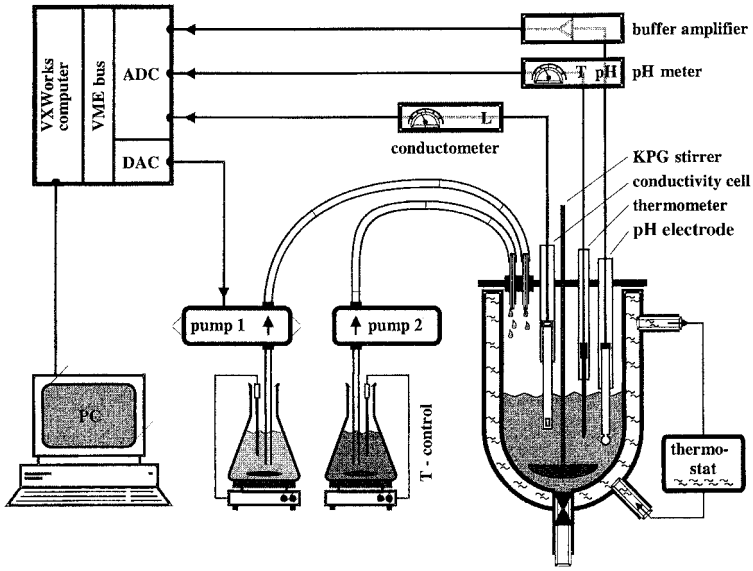

Figure 21. Scheme of the experimental set up used for the precipitation; for details refer to the text.

solutions yields constant pH samples. A computer-controlled installation has been used as shown in Figure 21 in order to achieve highest possible control over the precipitation process. The set-up consists of a thermostated reactor of 2000 mL volume equipped with a wing stirrer and a lid to minimize CO_2 exchange with the atmosphere. Ports are provided with fittings for the pH electrode (single junction, Schott BlueLine 13; temperature effect compensated by pH meter, voltage range -1.9 to 1.9 V), a conductivity electrode (WTW LF 530, 0–2 V) and a thermocouple (Pt-100 resistance thermometer). An on-line computer (VMEbus) provides via analog I/O interfaces an accurate control over the reaction in the tank. The interfaces are connected to the sensors using buffer amplifiers and to the pump supply (magnetically coupled toothed wheel pumps from Ismatec). A real time operating system (VxWorks) allows an isochronous handling of the process parameters. Process control is realized with a software-implemented PID algorithm allowing processing with a temporal resolution of 10 ms.

The concentrations of the solutions used were 1M with respect to the metals and 1.2M for $NaCO_3$. Each experiment was carried out with a total of 0.5 mol metals in the precipitate. The reaction container was thermostated to 65 °C and for the constant pH series filled prior to the precipitation with bidistilled H_2O (400 mL). The solutions of the metals were added at constant rates of 25 mL min^{-1}. The addition of the precipitation reagent was controlled as described above. The precipitates were aged for 120 min under continuous stirring at the precipitation temperature. The solids were washed after filtering six times each with bidistilled water (170 mL) whereby the suspension was stirred for 10 minutes at ambient temperature. Finally, the samples were dried at 120 °C in air for 20 h. In addition, different drying conditions were applied to test the influence on the final precursors. Samples with a Cu/Zn ratio of 70:30 were dried at 90 and 40 °C using a dew point dryer. Characterization by XRD and TG-MS revealed no verifiable differences to the standard sample.

To study the structural evolution during ageing a preparation at constant pH of composition 70:30 was conducted and specimens were taken at various times ranging from 3 min to 18 h. They were quenched from reaction temperature in an ice bath and no washing and drying was applied prior to X-ray analysis.

For the elemental analyses of the metals by AAS a Perkin–Elmer 4200 instrument was used. IR spectra were recorded with a FTIR Perkin Elmer 2000 using the KBr disc technique. XRD measurements were performed on a STOE STDI P instrument in Debye-Scherrer geometry equipped with a curved (45°) PSD. Samples were prepared in 0.3 mm capillaries to minimize texture effects. Thermal analyses were conducted on a NETZSCH STA449 thermobalance under a controlled flow of 40:10 mL min^{-1} N_2/O_2 with approximately 20 mg of the samples in open Al_2O_3 crucibles applying a heating rate of 10 K min^{-1}. The gases evolved in the thermal analyses were monitored with a quadrupole mass spectrometer (QMS200 Omnistar, Balzers) coupled to the thermal balance via a quartz capillary heated to 180 °C. The mass gates used were *m/e* 18 (H_2O), 28 (CO), 30 (NO), 32 (O_2), 44 (CO_2), and 46 (CO_2/NO_2). The signals of CO_2 and H_2O were quantified with calibration factors obtained by injections of known amounts of the gases using a GC injection system (capillary bypass of 0.5 mL). The accuracy of these values was checked by decomposition of weighted amounts of the reference materials $CaCO_3$ (Chempur, 99,9%) and $CuSO_4 \times 5H_2O$ (Merck, 99,9%) and found to agree within 1% of error. For the evaluation of the anionic composition calculated as mmol $M(OH)_2$ and MCO_3 per gram (with M being the mean molecular weight of the metals at the given Cu/Zn ratio) the CO_2 signal was used directly and the quantity of H_2O was split into contributions from $M(OH)_2$ and adsorbed water to account for the experimental weight loss. The composition was also calculated from the weight loss assuming that there are no other contributions besides CO_2 and H_2O. Both compositions agree within 1% with each other. With samples containing noticeable amounts of sodium salts such as those obtained after the first washing treatments this quantification procedure was not applied.

Acknowledgement

The help of G. Lorenz with the preparation is greatly acknowledged. We appreciate the fruitful discussions with Dr. T. Ressler and Dr. M. M. Günther relating our results to the structural properties of the catalyst.

[1] T. Matsuhisa in *Catalysis*: *A specialist periodical report*, *Vol. 12*, RSC, Cambridge, **1996**, p. 20.
[2] J. B. Bulko, R. G. Herman, K. Klier, G. W. Simmons, *J. Phys. Chem.* **1979**, *83*, 3118.
[3] P. L. Hansen, J. B. Wagner, S. Helveg, J. R. Rostrup-Nielsen, B. S. Clausen, H. Topsøe, *Science* **2002**, *295*, 2053.
[4] N.-Y. Topsøe, H. Topsøe, *J. Mol. Catal. A* **1995**, *141*, 95.
[5] Y. Kanai, T. Watanabe, T. Fujitani, M. Saito, J. Nakamura, T. Uchijima, *Catal. Lett.* **1994**, *27*, 67.
[6] L. M. Plyasova, T. M. Yur′eva, T. A. Kriger, O. V. Makarova, V. I. Zaikovskii, L. P. Solov'eva, A. N. Shmakov, *Kinet. Catal.* **1995**, *36*, 425.
[7] T. Fujitani, J. Nakamura, *Catal. Lett.* **1998**, *56*, 119.
[8] M. S. Spencer, *Catal. Lett.* **2000**, *66*, 255.
[9] M. M. Günter, T. Ressler, B. Bems, C. Büscher, T. Genger, O. Hinrichsen, M. Muhler, R. Schlögl, *Catal. Lett.* **2001**, *71*, 37.
[10] G. J. Millar, I. H. Holm, P. J. Uwins, J. Drennan, *J. Chem. Soc. Faraday Trans.* **1998**, *94*, 593.
[11] G.-C. Shen, S.-I. Fujita, S. Matsumoto, N. Takezawa, *J. Mol. Catal. A* **1997**, *124*, 123.
[12] R. W. Joyner, F. King, M. A. Thomas, G. Roberts, *Catal. Today* **1991**, *10*, 417.
[13] D. Waller, D. Stirling, F. S. Stone, M. S. Spencer, *Faraday Discuss. Chem. Soc.* **1989**, *87*, 107.
[14] P. B. Himelfarb, G. W. Simmons, K. Klier, R. G. Herman, *J. Catal.* **1985**, *93*, 442.
[15] G. J. de A. A. Soler-Illia, R. J. Candal, A. E. Regazzoni, M. A. Blesa, *Chem. Mater.* **1997**, *9*, 1984.
[16] P. M. Schosseler, B. Wehrli, A. Schweiger, *Inorg. Chem.* **1997**, *36*, 4499.
[17] P. Porta,S. de Rossi, G. Ferraris, M. Lo Jacono, G. Minelli, G. Moretti, *J. Catal.* **1988**, *109*, 367
[18] S. Ghose, *Acta. Crystallogr.* **1964**, *17*, 1051

[19] Sample from Chah Khuni, Iran with well developed crystals up to 5 mm. Identity and purity was checked by XRD.
[20] B. S. Rasmussen, P. E. H. Nielsen, J. Villadsen, J. B. Hansen, *Preparation of catalysts*, *Vol. IV*, Elsevier, Amsterdam, **1987** p. 785.
[21] A. M. Pollard, M. S. Spencer, R. G. Thomas, P. A. Williams, J. Holt, J. R. Jennings, *Appl. Catal. A* **1992**, *85*, 1
[22] R. S. W. Braithwaite, G. Ryback, *Mineral. Mag*. **1963**, *33*, 441.
[23] C. K. Huang, P. F. Kerr, *Am. Mineral*. **1960**, *45*, 311.
[24] pdf-file entry No. 14-687, International Centre for Diffraction Data, Newtown Square Corporate Campus, 12 Campus Blvd, Newtown Square, PA (USA) 19073-3273.
[25] a) H. Tanaka, S. Terada, *J. Thermal. Anal.* **1993**, *39*, 1011; b) J.-L. Li, T. Inui, *Appl. Catal. A* **1996**, *137*, 105.
[26] G. Sengupta, D. P. Das, M. L. Kundu, S. Dutta, S. K. Roy, R. N. Sahay, K. K. Mishra, S. V. Ketchik, *Appl. Catal.* **1989**, *55*, 165.
[27] I. M. Vasserman, N. I. Silant'eva, *Russ. J. Inorg. Chem.* **1968** *13*, 1041.
[28] B. Bems, unpublished results.
[29] S.-I. Fujita, A. M. Satriyo, G. C. Shen, N. Takezawa, *Catal. Lett.* **1995**, *34*, 85.
[30] T. M. Yurieva, *React. Kinet. Catal. Lett.* **1995**, *55*, 513.
[31] M. J. L. Gines, C. R. Apesteguia, *J. Thermal Anal.* **1997**, *50*, 745.
[32] M. M. Günther, B. Bems, R. Schlögl, T. Ressler, *J. Synchr. Rad.* **2001**, *8*, 619.
[33] M. M. Günther, T. Ressler, R. E. Jentoft, B. Bems, *J. Catal.* **2001**, *203*, 133.

Received: May 27, 2002
Revised: December 5, 2002 [F4122]

